

# **Insight into Flufenamic Acid Cocrystal Dissolution in the Presence of a Polymer in Solution: from Single Crystal to Powder Dissolution**

*Minshan Guo,<sup>†</sup> Ke Wang,<sup>†</sup> Ning Qiao,<sup>‡</sup> László Fábián,<sup>§</sup> Ghazala Sadiq,<sup>⊥</sup> and Mingzhong Li<sup>\*,†</sup>*

<sup>†</sup>School of Pharmacy, De Montfort University, Leicester, LE1 9BH, U.K.

<sup>‡</sup>College of Materials Science and Engineering, North China University of Science and  
Technology, Tangshan 063210, Hebei, China

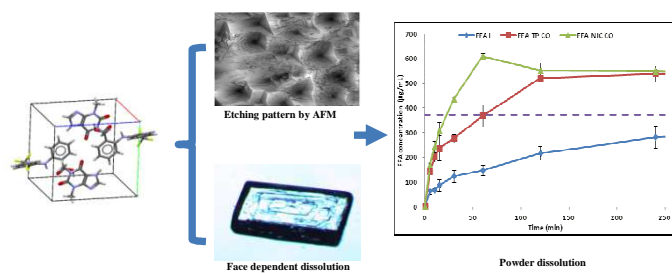
<sup>§</sup>School of Pharmacy, University of East Anglia, Norwich Research Park, Norwich, NR4 7TJ,  
U.K.

<sup>⊥</sup>The Cambridge Crystallographic Data Centre, 12 Union Road, Cambridge, CB2 1EZ, U.K.

---

\*Address: School of Pharmacy, De Montfort University, Leicester, LE1 9BH, U.K. Tel: +44-1162577132; Email: mli@dmu.ac.uk

## Table of contents (TOC)



**ABSTRACT:** Effects of three polymers, polyethylene glycol (PEG), polyvinylpyrrolidone (PVP), and copolymer of vinyl pyrrolidone/vinyl acetate (PVP-VA), on the dissolution behaviour of the cocrystals of flufenamic acid with theophylline (FFA-TP CO) and nicotinamide (FFA-NIC CO) were investigated at multiple length scales. At the molecular level, the interactions of crystal surfaces with a polymer were analysed by observing etching pattern changes using atomic force microscopy. At the macroscopic scale, dissolution rates of particular faces of a single crystal were determined by measurement of the physical retreat velocities of the faces using optical light microscopy. In the bulk experiments, the FFA concentration in a dissolution medium in the absence or presence of a polymer was measured under both sink and non-sink conditions. It has been found that the dissolution mechanisms of FFA-TP CO are controlled by the defect sites of the crystal surface and by precipitation of the parent drug FFA as individual crystals in the bulk fluid. In contrast, the dissolution mechanisms of FFA-NIC CO are controlled by surface layer removal and by a surface precipitation mechanism, where the parent drug FFA precipitates directly onto the surface of the dissolving cocrystals. Through controlling the dissolution environment by pre-dissolving a polymer, PVP or PVP-VA, which can interact with the crystal surface to alter its dissolution properties, improved solubility and dissolution rates of FFA-TP CO and FFA-NIC CO have been demonstrated.

**KEYWORDS:** cocrystal, polymer, flufenamic acid, dissolution, supersaturation, precipitation

## 1. INTRODUCTION

Pharmaceutical cocrystals have attracted remarkable interests for enhancing solubility and dissolution rates of poorly water soluble drugs.<sup>1-3</sup> A highly supersaturated solution concentration, which is significantly greater than the equilibrium saturation concentration of the parent drug, can be generated due to rapid dissolution of cocrystals, which is a key requirement for improved drug oral absorption.<sup>4</sup> However, maintaining such a supersaturated state is challenging because of the tendency for rapid precipitation of a more stable form of the parent drug during dissolution.<sup>5,6</sup> In order to maximise the potential of cocrystals, it is critical to include inhibitors in a formulation to prevent or delay the precipitation of the parent drug during dissolution.<sup>7-13</sup> Although polymeric crystallization inhibitors have been extensively studied in many other systems, in particular amorphous solid dispersions,<sup>14,15</sup> such studies are still rare for cocrystal based formulations. In a recent study, we have found that the competition of intermolecular hydrogen bonding among drug/coformer, drug/polymer, and coformer/polymer was a key factor responsible for maintaining the supersaturation through nucleation inhibition and crystal growth modification in a supersaturated cocrystal solution with a pre-dissolved polymer.<sup>11</sup> Therefore, selection of a polymeric excipient in a cocrystal formulation should consider the interplay of a polymer with both the parent drug and coformer in solution. On the other hand, it has to be stressed that pre-dissolved polymeric additives in solution can not only function as an inhibitor to maintain the supersaturated state of the parent drug, but also influence the dissolution properties of solid crystals. Therefore, the performance of cocrystal based products is determined by the overall effects of an inhibitor on both cocrystal dissolution and parent drug precipitation.

The process of crystal dissolution can be considered as specific types of heterogeneous reactions between the solid and solvent, in which solvent molecules are first adsorbed onto

the crystal surface.<sup>16</sup> Then, through interaction or reaction between the crystal and the adsorbed solvent molecules, the crystal molecules detach and diffuse away from the surface. Using atomic force microscopy (AFM), different etching patterns can be observed during crystal dissolution, affected by the crystal interaction network and the interactions between the crystal molecules in the lattice and solvent molecules.<sup>17-22</sup> When a polymer is present in solution, the polymer molecules can also be adsorbed on the surface of the dissolving crystal to form an adsorption layer, which affects solute bulk diffusion as well as surface diffusion. There are many factors affecting adsorption of a polymer on a crystal surface, such as properties of the polymer (i.e. polymer chains and chain rigidity) and crystal structure (i.e. molecular packing) and the adsorption energy involved in the specific interactions between the polymer and crystal surface,<sup>18,23-25</sup> For example, polyvinylpyrrolidone (PVP) and hydroxypropyl methylcellulose (HPMC) can slow down the intrinsic dissolution rate of acetaminophen crystals due to their strong interactions with the crystal surface through either van de Waals or hydrogen bonding interactions. In contrast, although the polymers poly(vinyl alcohol) (PVA) and poly(ethylene glycol) (PEG) can interact the crystal surface of acetaminophen through hydrogen bonding, they had no significant inhibitory effect on the dissolution and crystallization, because of high mobility of the functional groups.<sup>18</sup>

As a crystal dissolves, rates of dissolution of its faces are distinctly different due to their different interactions with the dissolution medium. A polar solvent is more likely to interact with polar crystal faces where polar atoms or functional groups are exposed normal to the faces.<sup>26</sup> Through measurement of the physical retreat rates of individual faces of a single crystal, a crystal surface dependent dissolution rate can be obtained, which can be used to determine the relationship between crystal morphology and bulk dissolution rates.<sup>27,28</sup> This knowledge of anisotropic dissolution behaviour of single crystals can highlight the factors

affecting crystal dissolution, which is crucial in the design, evaluation and control of therapeutic efficacy of solid dosage forms.<sup>29,30</sup>

Due to the complexity arising from the multi-component nature of pharmaceutical cocrystals, it is expected that the knowledge from single component crystals needs to be rigorously validated and further extended when applied to the dissolution of cocrystals. The present work, for the first time, is aimed at understanding the dissolution mechanisms of cocrystals in solution in the absence and presence of a pre-dissolved polymer. We carried out different dissolution experiments of both single and power cocrystals to examine the dissolution properties at multiple length scales. At the molecular level, we investigated how a cocrystal surface interacted with a polymer by analysing the etching pattern changes observed by AFM. At the macroscopic scale, dissolution rates of particular faces of a single crystal were determined by measurement of the physical retreat velocities of different faces using optical light microscopy (OLM). In the bulk experiments, the concentration of a drug in a dissolution medium in the absence or presence of a polymer was measured under both sink and non-sink conditions and the dissolution rate was deduced from the evolution of this concentration. Sink condition experiments were performed to evaluate the effect of a polymer on the dissolution rate of cocrystals, and non-sink condition ones to evaluate the ability of a polymer to generate and maintain supersaturated drug solutions. Under sink conditions the change of a cocrystal dissolution rate during dissolution should be directly related to the interaction between the pre-dissolved polymer in solution with the dissolving crystal surface. Evaluation of the supersaturating systems benefits from the use of non-sink conditions that mimic the in vivo conditions in the gastrointestinal tract. The cocrystals of flufenamic acid-nicotinamide (FFA-NIC CO) and flufenamic acid-theophylline (FFA-TP CO) with three chemically diverse polymers, polyethylene glycol (PEG), polyvinylpyrrolidone (PVP), and copolymer of vinyl pyrrolidone/vinyl acetate (PVP-VA) were selected, with the aim to

identify the different influences of these polymers on cocrystal dissolution. The chemical structures of the model drug, the coformers, and the monomer units of the polymers are shown in Table 1 and their detailed description can be found in our previous publication.<sup>11</sup> In order to eliminate the effect of viscosity, a low polymer concentration of 200  $\mu\text{g/mL}$  was used in the study. At this polymer concentration the equilibrium solubility of FFA remained virtually the same as without the presence of the polymers. Because of the thermodynamically unstable nature of a cocrystal in solution, the solubility of FFA-TP CO and FFA-NIC CO was determined by their eutectic points through measuring their solubility curves.<sup>31</sup> The faces of FFA I (flufenamic acid form I), FFA-TP CO and FFA-NIC CO single crystals were indexed using X-ray diffraction and nanometre-scale models of their morphologies which were created using Mercury 3.9 (The Cambridge crystallographic Data Centre, Cambridge, UK). These morphology models were also used to explain the properties of each face of a single crystal in the AFM and OLM dissolution experiments. In order to quantify the effect of a pre-dissolved polymer on the powder dissolution performance, the dissolution performance parameters (DPPs) in different non-sink condition experiments were calculated and compared. The solid residues after the solubility and powder dissolution experiments were examined by differential scanning calorimetry (DSC), powder X-ray diffraction (PXRD) and Fourier transform infrared spectroscopy (FTIR).

## 2. MATERIALS AND METHODS

**2.1. Materials.** Flufenamic acid form I (FFA I), nicotinamide (NIC) ( $\geq 99.5\%$  purity), theophylline (TP) ( $\geq 99.5\%$  purity), potassium dihydrogen phosphate ( $\text{KH}_2\text{PO}_4$ ) and sodium hydroxide (NaOH) were purchased from Sigma-Aldrich (Dorset, UK). Poly(ethylene glycol) 4000 (PEG) was purchased from Sigma-Aldrich (Dorset, UK). Plasdone K-29/32 (PVP) and Plasdone S-630 copovidone (PVP-VA), which is a 60:40 copolymer of N-vinyl-2-pyrrolidone and vinylacetate, were gifts from Ashland Inc. (Schaffhausen, Switzerland). Methanol (HPLC

grade) and acetonitrile (HPLC grade) were purchased from Fisher Scientific UK (Loughborough, UK) and used as received. Double distilled water was generated from a Bi-Distiller (WSC044.MH3.7, Fistreem International Limited, Loughborough, UK) and used throughout the study.

**2.2. Methods.** *0.01M pH 6.8 Phosphate Buffer Solution (PBS).* In this study 0.01 M pH6.8 PBS was prepared as a dissolution medium according to British Pharmacopeia 2010. 50 mL of 0.2 M potassium dihydrogen phosphate ( $\text{KH}_2\text{PO}_4$ ) and 22.4 mL of 0.2 M sodium hydroxide (NaOH) were mixed and diluted to 1000 mL with double distilled water.

*Powdered FFA Cocrystals.* Cocrystals of FFA-NIC CO and FFA-TP CO were prepared by solvent evaporation and cooling crystallization methods respectively, as detailed in our previous publication.<sup>11</sup> Formation of cocrystals was confirmed by DSC, FTIR and PXRD.

*Single FFA Cocrystals.* Single crystal of FFA I was directly selected from the commercial products while the single cocrystals of FFA-NIC CO and FFA-TP CO were grown from a saturated 1:1 equimolar mixture solution of FFA and coformers in cosolvent (7:3 mixture of acetonitrile and water) by slow evaporation at room temperature over a period of 3-4 days. FFA cocrystals were harvested by vacuum filtration of the mother solutions. The phase identities of the single crystals were confirmed by DSC, FTIR and PXRD.

*Single Crystal Face Indexing and Morphology Models.* To identify the exposed crystal faces during AFM and OLM dissolution experiments, representative crystals of each type were mounted on an Oxford Diffraction XCalibur diffractometer. Only a few X-ray images were collected for each crystal, which allowed determination of the unit cell parameters and the orientation matrix. The major faces could then be identified by orienting the crystals in specific crystallographic directions on the diffractometer, while observing them through the built-in camera. Models of the observed morphologies were created in Mercury 3.9 (The Cambridge crystallographic Data Centre, Cambridge, UK) by manually adjusting the list of

faces and face-to-centroid distances to match those observed experimentally on the diffractometer. A summary of these results is given in Figure 2, with the single crystal indexing data in Table S1 in the supplementary materials.

*Apparent Equilibrium Solubility of FFA I.* Apparent equilibrium solubility of FFA I was measured by adding excess amount of crystalline materials into a small vial with 20 mL of 0.01 M pH 6.8 PBS with or without 200 µg/mL of a polymer (PEG, PVP or PVP-VA) in a shaking water bath at 250 RPM sharking rate and 23±0.5°C for 24 h. The suspension was separated by an MSB 010.CX2.5 centrifuge (MSE Ltd, London, UK) at 1.3 x 10000 RPM for 1 min. The FFA concentration was determined by HPLC. The solid residuals retrieved from tests were analysed by DSC, FTIR, and PXRD. All tests were repeated in triplicate.

*Cocrystal Solubility.* For a 1:1 cocrystal of AB without consideration of ionization of each component, its solubility is calculated as,<sup>31</sup>

$$S_{AB} = \sqrt{K_{sp}} = \sqrt{A_{eu}B_{eu}} \quad (1)$$

where  $K_{sp}$  is the solubility product of the AB cocrystal and concentrations of  $A_{eu}$  and  $B_{eu}$  are transient concentrations of drug and coformer where the solution is in equilibrium with solid drug and cocrystal.

In order to measure the transition concentrations of FFA and a coformer of TP or NIC in PBS, a series of the coformer solutions were prepared: 0, 7.1, 8.9, 10.7, 12.4, 14.2 mmol/L for TP solutions and 0, 17.8, 57.4, 61.8, 66.2, 71.1, 142.3 and 213.4 mmol/L for NIC solutions. Excess amount of FFA I crystalline materials was added into a small vial with 20 mL of each of the prepared coformer solutions in a shaking water bath at 250 RPM sharking rate and 23±0.5°C for 24h. The concentrations of FFA and coformer of TP or NIC were determined by HPLC and the solid residues retrieved were analysed by PXRD, DSC, and FTIR. The transition concentrations (or a eutectic point) of a cocrystal were determined in the

lowest coformer solution prepared where two solid phases of the solid drug and cocrystal coexisted in equilibrium with solution. All experiments were repeated in triplicate.

*Atomic Force Microscopy (AFM) Measurements.* Single crystals with well-defined and visually flat faces were selected for dissolution study. In order to correlate the etching pits with the crystal structure, the axis directions were determined by comparing the observed crystal face with the indexed crystal morphology created by Mercury 3.9. A single crystal was first mounted onto an AFM sample disk using double-sided seal tape, in which the studied face was up. The prepared sample disk was then immersed in a petri dish with 20 mL of 0.01 M pH 6.8 PBS in the absence or presence of a polymer at room temperature for a period of time varying from 2 min to 10 min as shown in Table 3. After a predetermined time interval, the disk was taken from the solution and the remaining solution on the crystal surface was removed with filter paper. Finally, the sample was air-dried for at least 0.5 h before AFM observation.

The surfaces of single crystals of FFA I, FFA-TP CO and FFA-NIC CO before and after the immersing dissolution tests [Table 3] were observed with an AFM (Agilent 5420 SPM, USA). AFM measurements were carried out in contact mode at room temperature using a J-type piezo-scanner with a standard silicon nitride tip (Windsor Scientific Ltd, UK). The resolution of a measurement was 512×512 points with equal steps along the x and y directions. Three scans on the same area were conducted at 80×80  $\mu\text{m}^2$ , 40×40  $\mu\text{m}^2$ , and 20×20  $\mu\text{m}^2$  for single crystals of FFA I and FFA-TP CO and 40×40  $\mu\text{m}^2$ , 20×20  $\mu\text{m}^2$ , and 10×10  $\mu\text{m}^2$  for single crystals of FFA-NIC CO. The images created by AFM system software were saved as the deflection mode, which was the derivative along the scan directions of the surface profile.

*Optical Light Microscopy (OLM) Dissolution Monitoring for Single Crystals of FFA I and FFA COs.* A LEICA DM 750 polarized light microscope (Leica Microsystem Ltd,

Milton Keynes, UK) with video camera at 200x magnification and version 4.0 of the Studio Capture software were used to monitor the displacement of different faces of a single crystal during dissolution. A single crystal was horizontally placed inside a petri dish with one end fixed by blue tack and then followed by addition of 20 mL of PBS in the absence or presence of a 200 µg/mL pre-dissolved polymer. Data were collected at 0 h, 2 h, 4 h and 6 h.

*Powder Dissolution Tests.* Powder dissolution experiments of FFA I, FFA-TP CO and FFA-NIC CO were performed under both sink and non-sink conditions. All crystalline materials prior to the tests were slightly ground by a mortar and pestle and sieved by a 60 mesh sieve (below 250µm) to reduce the effect of particle size on the dissolution rates. 400 mL of 0.01M pH 6.8 PBS in the absence or presence of 200 µg/mL of a polymer (i.e., PEG, PVP or PVP-VA) in a flat bottom beaker was used in each of the experiments. Cocrystal powders with equivalent 40 mg of FFA I were used for the sink condition experiments, while powders with equivalent 400 mg of FFA I were used for non-sink condition tests. The dissolution tests were conducted at  $23\pm0.5^{\circ}\text{C}$  with the aid of magnetic stirring at 250 RPM. Samples of  $1\pm0.1$  mL were withdrawn from the dissolution vessel at predefined time points of 5, 15, 30, 60, 120 and 240 min and analysed by HPLC to determine the concentrations of FFA and coformer NIC or TP. Solid residues retrieved from the non-sink condition experiments were dried at room temperature and analysed by DSC, FTIR and PXRD. All experiments were repeated in triplicate.

*Dissolution Performance Parameter (DPP).* Dissolution performance parameter (DPP), analogous to the supersaturation parameter in our previous publication,<sup>11</sup> was used to evaluate the dissolution profile of cocrystal powders in the absence or presence of a pre-dissolved polymer in comparison to a reference system. Figure 1 shows the dissolution profiles of different solid powers in which  $C_{\text{equilibrium}}$  is the equilibrium drug concentration in the dissolution medium. The area under the curve (AUC)  $AUC_{C(t)}$  of a dissolution profile  $C(t)$

indicates the amount of drug dissolved and is maintained over the period of the dissolution time from 0 to t. A higher AUC of the dissolution profile indicates a better dissolution performance. A curve  $C_R(t)$  is the reference dissolution profile of solids  $R$  with  $AUC_{C_R(t)}$ . For solid A with a dissolution curve  $C_A(t)$ , its concentration passes the equilibrium value at  $T_{equilibrium}$  and reaches the maximum  $C_{A\_max}$ . The  $AUC_{C_A(t)}$  is significantly higher than that of the reference solids R, indicating more of solid A dissolves. Compared with the reference solid R, the solid B dissolves less, because of a smaller value of  $AUC_{C_B(t)}$ . In order to quantitatively compare the dissolution performance of two solids, DPP is defined as

$$DPP = \frac{AUC_{C(t)} - AUC_{C_R(t)}}{AUC_{C_R(t)}} \times 100\% \quad (2)$$

Solids with a positive DPP value have an increased ability to dissolve and to be maintained in a dissolution medium, while as a negative DPP value indicates that solids have a less ability to dissolve and to be maintained in solution.

*High Performance Liquid Chromatography (HPLC) Analysis.* The concentration of FFA, NIC or TP in solution was determined by Perkin Elmer series 200 HPLC (PerkinElmer Ltd, Beaconsfield, UK) with a HAILL 100 C18 column (5  $\mu$ m, 250  $\times$  4.6 mm) (Higgins Analytical Inc., Mountain View, CA, USA) at ambient temperature. An isocratic method was used with 15% water (including 0.5% formic acid) and 85% methanol at 1.5 mL/min flow rate and 286 nm wavelength was used for detecting FFA concentration. Both NIC and TP concentrations were identified by an isocratic method with 55% methanol and 45% water at 1mL/min flow rate and 265 nm.

*Differential Scanning Calorimetry (DSC).* A PerkinElmer Jade DSC (PerkinElmer Ltd., Beaconsfield, UK) was employed to characterize the melting points of solids. 8-10 mg of the samples was added into a crimped aluminium pan with a pinhole pierced lid for testing at 20°C/min heating rate under a nitrogen flow rate of 20 mL/min. The temperature range of

FFA I, NIC and FFA-NIC cocrystal was 25°C to 250°C while for TP and FFA-TP cocrystal it was 25°C-320°C.

*Powder X-ray Diffraction (PXRD).* Powder X-ray patterns of solids was recorded from 5° to 35° at a scanning rate of 0.3° (2 $\theta$ ) min<sup>-1</sup> by a D2 PHASER diffractometer (Bruker UK Limited, Coventry, UK). Solids of FFA I and FFA cocrystals were crushed using a mortar and pestle before the measurements. Cu-K $\alpha$  radiation was used with a voltage of 30 kV and a current of 10 mA. The calculated PXRD patterns of solid powders were obtained utilizing Mercury (The Cambridge Crystallographic Data Centre, Cambridge, UK).

*Fourier Transform Infrared Spectroscopy (FTIR).* An ALPHA interferometer (Bruker UK Limited, Coventry, UK), equipped with a horizontal universal attenuated total reflectance (ATR) accessory, was used to measure the FTIR spectra of solid samples. For each of the samples, 30 scans were collected per spectrum with a resolution of 2 cm<sup>-1</sup> in the spectral region of 400 to 4000 cm<sup>-1</sup> using the OPUS software. All the spectral data were collected at an ambient temperature.

### 3. RESULTS

**3.1. FFA I and FFA Cocrystals Characterization, Morphology Prediction and Face Indices.** Single cocrystals of FFA-NIC CO and FFA-TP CO were grown using the slow solvent evaporation technique described in the Materials and methods section. The identities of the crystals have been confirmed by PXRD, DSC and FTIR measurements [See Figure S1 in the supplementary materials]. Single FFA-NIC COs harvested were thin, brick-shaped and single FFA-TP COs were chunky, with sizes ranging from millimetres up to one centimetre. The single crystals of FFA I from the received materials were plate-like with a wider size range from millimetres up to one centimetre. Representative microscopy images of these single crystals are shown in Figure 2.

Models of the crystal morphologies were created using Mercury 3.9 based on the crystal structures of each material obtained from the Cambridge Structural Database (CSD refcodes: FPAMCA18 for FFA I; EXAQAW for FFA-NIC CO; ZIQDUA for FFA-TP CO, detailed in Table S1 in the supplementary materials) and face indexing of representative single crystals using an X-ray diffractometer [Section 2.2, Figure 2].

The FFA I structure is formed with hydrogen-bonded dimers between the carboxyl groups of two FFA molecules.<sup>32</sup> In the FFA-NIC CO structure, hydrogen-bonded rings are formed by two FFA and two NIC molecules. These four-molecule rings are linked into infinite tubes by the amide chain motif.<sup>33</sup> Regarding the FFA-TP CO structure, TP molecules form a dimer via N-H $\cdots$ O hydrogen bonds involving the saturated N atom of the imidazole ring and one of the carbonyl groups. An O-H $\cdots$ N hydrogen bond involving the carboxylic acid of the FFA and unsaturated N atom of the imidazole ring of TP results in a four-component supramolecular unit.<sup>34</sup> The identity of each powder sample was confirmed by comparison of the measured and predicted PXRD patterns shown in Figure 2. It can be seen that the calculated PXRD patterns were in good agreement with the experimental data for all crystals. All main PXRD peaks of FFA I were predicted accurately. Some mismatched peak positions in the predicted and measured PXRD patterns of cocrystals of FFA-NIC CO and FFA-TP CO were found in Figure 2 (indicated by arrows). These differences were likely to come from the different temperatures of the measurements, i.e., room temperature for PXRD measurements and around 100 K for the single crystal data.<sup>33,34</sup> At different temperatures the size of the unit cell will be (slightly) different, leading to the shifts of the PXRD peak positions.

In comparison with the observed single crystal images in Figure 2, it can be seen that the crystal morphologies of FFA I, FFA-TP CO and FFA-NIC CO are represented accurately by

the models created by the software of Mercury 3.9. Therefore each surface of a single crystal can be assigned through directly comparing the measured image with its morphology model.

Six well-defined planes of a single FFA I crystal were identified, with a pair of major faces, (100) and (-100), bounded by two pairs of the less prominent side faces (011), (0,-1,-1), (01-1) and (0-11). The (100) plane could expose either the COOH or the CF<sub>3</sub> groups [Figure 2]. The (0-11) face, on the other hand, exposes the COOH and CF<sub>3</sub> groups simultaneously, along with the aromatic rings [Figure 2]. Based on this structural inspection, it is expected that subsequent (100) layers with dominant CF<sub>3</sub>...CF<sub>3</sub> contacts should have lower attachment energy than the (0-11) faces and have a slow growth rate normal to the surface, leading to a large face.

The rectangular shape of FFA-TP CO is formed with a pair of the dominant (001) and (00-1) faces, larger side faces (0-10) and (010), and smaller side faces (100) and (-100). The (001) face could again have a more hydrophobic nature, because the trifluoromethylbenzene rings of FFA are exposed almost perpendicularly out of this surface. In contrast, the crystal faces (0-10) and (100) are more hydrophilic, because they expose more hydrogen-bond donors and acceptors.

The dominant pair of FFA-NIC CO faces are (0-11) and (01-1), with less prominent faces (011) and (0-1-1) and the smallest pair of (-100) and (100). On the (100) face, both COOH groups of FFA and CONH<sub>2</sub> groups of NIC are exposed, resulting in a polar surface. The (01-1) plane is less polar, carbon, fluorine and hydrogen atoms are dominating the exposed area.

**3.2. Solubility Study.** The apparent FFA I equilibrium solubility at 23°C was 373.3±4.2 µg/mL in PBS and was comparable of those of FFA I in the presence of 200 µg/mL PEG (376.3±6.7 µg/mL), PVP (387.7±5.9) or PVP-VA (398.8±2.3 µg/mL) shown in Table 2, indicating that none of the polymers changed the equilibrium solution properties. The solid

residues collected after the experiments were analysed by DSC, FTIR and PXRD, and indicated that they were the same as the starting materials [Figure S2, supplementary materials].

The concentrations of FFA and TP after equilibration for 24 h when excess amount of FFA I was added into each of the prepared TP solutions are shown in Figure 3(a). The solubility of FFA I initially increased slightly with increasing the TP concentration due to soluble complex formation between the two compounds. When the TP concentration exceeded 8.9 mM, it was found that the apparent solubility of FFA I reached a plateau, because the solubility limit of the complex formed was exceeded and the concentration of uncomplexed FFA in solution did not change significantly. Only an averaged 1.2-fold increase in the apparent solubility of FFA I was observed in the presence of TP in comparison to FFA I solubility in PBS alone. Precipitation of the FFA-TP CO was observed based on PXRD analysis [DSC and FTIR results in Figure S3 in the supplementary materials] of the solid residues, which indicated the presence of two solid phases, FFA-TP CO and FFA I as shown in Figure 3(b). Therefore, the measured concentrations of FFA and TP in this solution represent the FFA-TP CO transition concentration [Table 2]. The molar ratio of FFA to TP at the transition point was 0.26:1, indicating that the system is incongruently saturating. The solubility of FFA-TP CO was calculated as 2.99 mmol/mL using Equation (1), which is a 2.25-fold increase compared to the solubility of FFA I alone.

The apparent concentration of FFA I as a function of NIC concentration is shown in Figure 3(c), which is similar to a previous work.<sup>8</sup> The apparent solubility of FFA I increased with increasing NIC concentration up to 61.8 mM, indicating complex formation of FFA and NIC in solution. In this region, the solubility limit of the complex formed was not exceeded, therefore the solid residues were FFA I alone, confirmed by PXRD results in Figure 3(d) [DSC and FTIR results in Figure S4 in the supplementary materials]. In solutions with a NIC

concentration of 66.8 mM or above, the solid residues indicated the presence of two phases: FFA-NIC CO and FFA I solids, again confirmed by PXRD results in Figure 3(d) [DSC and FTIR results in Figure S4 in the supplementary materials]. Therefore the measured concentrations of FFA and TP in the 66.8 mM NIC solution represent the FFA-NIC CO transition concentration shown in Table 2. The molar ratio of FFA to NIC at the transition point was 0.026:1. The solubility of FFA-NIC CO was determined to be 10.4 mM, which is a 7.83 fold increase compared to the solubility of FFA I alone.

**3.3. AFM Measurements of Single Crystals.** Figure 4 shows the representative AFM images of the faces of single crystals at a  $40 \times 40 \mu\text{m}^2$  scan area after exposure to PBS in the absence and presence of PEG, PVP, or PVP-VA. The AFM images at other scans can be found in Figure S5 in the supplementary materials. Before the etching experiments, the surfaces of FFA I and FFA-TP CO studied were generally flat and smooth, but with clear defects shown in Figures. 4(a) and (f). In contrast, the FFA-NIC CO (01-1) face was not smooth, but was marked with many parallel strips.

After being etched by PBS, clear etching patterns appeared on the FFA I (100) face shown in Figure 4(b). The pits observed were roughly circular in shape and were randomly distributed on the surface. Their diameters ranged from  $1 \mu\text{m}$  to  $10 \mu\text{m}$  with depths of up to  $0.5 \mu\text{m}$  shown in three dimensional AFM images in Figure S6 in the supplementary materials. When the FFA I (100) face was etched using PBS in the presence of PEG, bigger and deeper pits were obtained in comparison with those etched by PBS alone [Figure 4(c) and Figure S6]. Similar pits were also obtained by etching in the presence of PVP, but they appeared at a much smaller in diameter. In contrast, the pattern etched by PBS in the presence of PVP-VA was less regular, with pits of varied shapes and sizes.

When the FFA-TP CO (001) face was etched by PBS, many small interpenetrating trapezium pits with some isolated pits were formed with diameters of less than  $1 \mu\text{m}$  [Figure

4(g)]. At the same time, several long ditches were observed, with depth of about 1.3  $\mu\text{m}$  [Figure S6]. In the presence of PEG in PBS, similar etching patterns were obtained to that etched by PBS alone [Figure 4(h)]. The sizes of the well-defined separate pits in Figure 4(i), etched by PBS in the presence of PVP, were much larger than those by PBS alone or in the presence of PEG. The etching pattern by PBS in the presence of PVP-VA, shown in Figure 2(j), was very different, with less clearly defined ditches than in PBS alone.

The etching patterns in Figure 4(i)-(o) on the FFA-NIC CO (01-1) face etched by PBS in the absence and presence of PEG, PVP or PVP-VA were very similar to the original surface [Figure 4(k)], showing striped patterns with lines in the direction of the *a*-axis. However, the roughness of the FFA-NIC CO (01-1) face was different after etching dissolution in different dissolution media in Figure S6 in the supplementary materials. In PBS with the pre-dissolved PVP-VA the roughness of the etching surface is pretty much same as the original one while the surface is roughest etched by PBS in the pre-dissolved PEG.

**3.4. Face Dissolution Rate Determination of Single Crystals.** The temporal change in the lateral dimensions of a single crystal was recorded by measurements of the retreating face using OLM. The measurements were made for two faces of each single crystal: (100) and (0-11) faces of FFA I, (001) and (100) faces of FFA-TP CO and (01-1) and (100) faces of FFA-NIC CO.

Representative images of a single crystal during dissolution recorded by OLM are shown in Figure 5(a) [all other images can be found in Figure S7 in the supplementary materials] and the face dissolution profiles of each single crystal are shown in Figure 5(b). A linear relationship for different faces of both FFA I and FFA-TP CO single crystals in PBS in the absence or presence of a polymer was observed in Figures 5(b1)-(b8), indicating a constant dissolution rate. The face dependent dissolution rate was determined from the gradient of a plot of displacement of the edge of a face versus dissolution time. It can be seen in Figure 6

that the dissolution rates of different faces for the same crystal are distinctly different. It was found that for the same crystal the bigger face had a lower dissolution rate. In the presence of PEG in PBS, the dissolution rates of the faces of FFA I or FFA-TP CO increased slightly except the FFA-TP CO (100) face, indicating PEG can enhance the crystal dissolution. In contrast, in the presence of PVP or PVP-VA, the retreating rates of the faces of FFA I or FFA-TP CO decreased, indicating PVP or PVP-VA can retard the face dissolution.

FFA-NIC CO shows complicated face dependent dissolution behaviour in Figures. 5(b9)-(b12). In contrast to FFA I and FFA-TP CO, the dissolution rate increased rapidly on both of faces in the presence of PVP or PVP-VA in PBS. The variation of the dissolution rate on the small (100) face was significantly higher than the big face (01-1). It was interesting to note that the pre-dissolved PEG in solution decreased the dissolution of the small face (100) and increased the dissolution of the big face (01-1), leading to close to isotropic dissolution behaviour of FFA-NIC CO faces. Furthermore, only FFA-NIC CO faces showed good linear dissolution behaviour in PBS in the presence of a polymer of PEG.

**3.5. Powder Dissolution Under Sink and Non-Sink Conditions.** Figure 7 shows the dissolution profiles of FFA I, FFA-TP CO and FFA-NIC CO in the absence and presence of a polymer under sink conditions in which  $C_{equilibrium}$  was 100  $\mu\text{g/mL}$  (based on all the materials dissolved in solution). The gradient of a dissolution curve indicates the solid dissolution rate. Without a pre-dissolved polymer in solution, FFA-TP CO was shown to dissolve fastest, with 24% increase of AUC in comparison with that of pure FFA I solids. FFA-NIC COs dissolved rapidly in the first 5 min, but after that their dissolution rate slowed and became comparable with FFA I, indicating that a phase transformation to FFA occurred. Overall the AUC of FFA-NIC COs was 11% higher than that of FFA I. There was no significant change (within  $\pm 2\%$ ) of DPP and dissolution rate of FFA I, FFA-TP COs or FFA-NIC COs in the pre-dissolved PEG solution. With pre-dissolved PVP or PVP-VA, the

dissolution performance of FFA-NIC COs improved remarkably, i.e., in the pre-dissolved PVP solution 75% of solids dissolved within 15 min and AUC increased by 34%, while in the pre-dissolved PVP-VA solution 89% of solids dissolved within 15 min and AUC increased by 38%. In contrast, both PVP and PVP-VA reduced the dissolution rate and DPP of FFA-TP COs and FFA I solids as shown in Figure 7(e).

Figure 8 shows the dissolution profiles of FFA I, FFA-TP CO and FFA-NIC CO in the absence and presence of a polymer under non-sink conditions. Therefore  $C_{equilibrium}$  was the FFA I solubility of 373.3  $\mu\text{g/mL}$  measured in this study in Table 2.  $T_{equilibrium}$  and  $C_{max}$  values of each test are shown in Tables 4 and 5. In the presence of a polymer, FFA I solids dissolved slower [Table 4], in particular, the pre-dissolved PVP lead to 38% reduction of AUC in Figure 8(e). There was no supersaturation generated from FFA I dissolution in PBS in the absence or presence of PEG, PVP or PVP-VA [Table 5]. FFA-TP COs show an advantage of improved dissolution relative to FFA I solids both in the absence or presence of a pre-dissolved polymer. Pre-dissolved PVP can modestly increase the DPP of FFA-TP COs, to 40% from 30% in pure PBS, while pre-dissolved PVP-VA can slightly decrease its DPP to 24%. A significant increase of DPP of FFA-TP COs, to 56%, was observed in the pre-dissolved PEG. Pre-dissolved PEG in PBS can increase the dissolution rate of FFA-TP CO, showing a reduced  $T_{equilibrium}$  in contrast to the slow FFA-TP CO dissolution in the presence of PVP or PVP-VA in PBS [Table 4]. There was no dissolution advantage observed for FFA-NIC COs in PBS alone or in the presence of pre-dissolved PEG. However, in the presence of PVP in the solution, the advantage of FFA-NIC COs in dissolution performance was apparent, with a 64% increase of AUC [Figure 8(e)], 50% higher peak solubility [Table 5], and faster dissolution rate [Table 4]. Similarly, in the presence of PVP-VA in solution, the DPP of FFA-NIC COs was increased by 60% and the maximum FFA concentration was 1.6 times of its solubility.

The PXRD results of the solid residues collected after the FFA I dissolution experiments were the same as for the starting materials, shown in Figure 9(a), indicating that there was no phase transformation for FFA I in solution. The solid residues from the FFA-NIC CO experiments in the presence or absence of a pre-dissolved polymer gave PXRD patterns [Figure 9(c)] that matched the characteristic features of FFA III,<sup>35</sup> indicating that FFA III crystals precipitated during dissolution. Interestingly, in the presence of PVP or PVP-VA, the solid residues after the FFA-TP CO dissolution tests were their starting materials, FFA-TP COs, as shown in Figure 9 (b). In contrast, the solid residues after FFA-TP CO dissolution tests in PBS or in the presence of pre-dissolved PEG were the mixtures of FFA-TP CO and FFA III solids. The DSC and FTIR results of the solid residues are shown in Figure S8 and Figure S9 in the supplementary materials

#### 4. DISCUSSION

It is well known that the dissolution mechanism of the cocrystals of poorly water soluble drugs is complex, in which both dissolution of the cocrystals and the precipitation of the parent drug can occur simultaneously depending on the properties of the parent drug and coformer and the experimental conditions.<sup>5</sup> In this study, through rational selection of a coformer as well as the dissolution medium in the presence of a polymeric additive, we aimed to provide mechanistic insights into the intrinsic relationship among dissolution, supersaturation and precipitation for pharmaceutical cocrystals.

Based on the measured transition concentrations of the parent drug FFA I and coformers of NIC and TP, it was shown that FFA-NIC CO increased the FFA solubility by 7.83 fold, while the increase was 2.25 fold for FFA-TP CO. Discrepancies between predicted and observed solubility advantages were significant in the bulk experiments. In the powder dissolution experiments FFA-TP CO partially revealed its solubility advantage in PBS. Under sink conditions [Figure 7(a)] it showed 24% increase of AUC and under non-sink conditions

[Figure 8(a)] achieved a maximum FFA concentration of 497.5  $\mu\text{g/mL}$ , which was just 1.33 fold of its parent drug solubility. Despite having a higher solubility, FFA-NIC CO dissolved slower than FFA-TP CO in PBS under either sink or non-sink conditions [Figure 7(a), Figure 8(a)]. However, when PVP or PVP-VA was pre-dissolved in the dissolution medium, the expected improvements in dissolution rate and apparent FFA concentration were clearly revealed in the bulk dissolution experiments of FFA-NIC CO shown in Figures. 7(c)-(d) and Figures. 8(c)-(d). In contrast, under non-sink conditions the dissolution rate of FFA-TP CO decreased with slightly higher  $C_{max}$  in the presence of PVP or PVP-VA relative to dissolution in PBS without a polymer.

Based on the crystal structure illustrated in Figure 2, it is shown that the hydrogen bonding between the FFA and NIC molecules creates a layer structure of the crystal lattice where the NIC molecules form channels among the FFA molecules. Such configuration in the crystal lattice allows complete layers of molecules to be easily removed from the surface by the solvent medium.<sup>36</sup> Therefore the etching surface shown in Figure 4(i) of the FFA-NIC CO (01-1) face etched by PBS was almost same as the initial surface Figure 4(k). Due to rapid removal of the hydrophilic NIC molecules from the surface during dissolution, a local supersaturation of FFA near the dissolving surface of FFA-NIC CO was generated, leading to precipitation of the stable form FFA solids on the cocrystal particle, indicating changes in the roughness of the etching surface [Figure S6] observed by AFM. Consequently this resulted in reduction of the dissolution rate of FFA-NIC CO. Therefore, the dissolution profile of FFA-NIC CO was similar to FFA I, which was observed in the bulk powder dissolution in Figure 8(a). It has been reported that FFA has up to nine different crystal forms, among which FFA I (white colour) and FFA III (yellow colour) are the most commonly encountered.<sup>35</sup> Below a temperature of 42°C FFA III is the most stable form and has a lower solubility than its metastable form of FFA I, although the solubility difference between the two forms is very

small with less than 1  $\mu\text{g/mL}$ .<sup>37</sup> Precipitation of the solid FFA III during dissolution under non-sink conditions shown in Figure 9(c) demonstrated that the supersaturation was first generated by the FFA-NIC CO dissolution and then followed by precipitation of the stable form FFA III. Furthermore, a nonlinear relationship of the concentration vs time data acquired for the FFA-NIC CO (01-1) face in Figure 5(b) also concluded precipitation of FFA solids on the dissolving crystal surface. In contrast, no supersaturation was generated by dissolution of FFA I crystals, confirmed by the PXRD results in Figure 9(a) where the solid residues collected after the FFA I dissolution tests were the same as the starting materials.

According to the FFA-TP CO structure shown in Figure 2, an extended chain structure formed by a supramolecular ladder network involving both FFA and TP molecules with a strong hydrogen bond and interactions of  $\text{C-H}\cdots\pi$  and  $\pi\cdots\pi$  implies that the stronger crystal lattice of FFA-TP COs hinders surface dissolution and hence impacts the overall solubility. However, each surface of a FFA-TP CO becomes more hydrophilic due to inclusion of TP molecules in the crystal lattice in comparison with those of FFA I shown in Figure 2, leading to an increased interaction force between the faces of FFA-TP COs and aqueous solvent molecules. Therefore, FFA-TP CO has a limited ability to improve the FFA solubility by 2.25 fold in Table 2. Similarly to the parent drug FFA I, the dissolution mechanism of FFA-TP COs appears to be controlled by defect locations on the crystal surface and the underlying crystal lattice. Because the molecules at defect sites have higher mobility to be detached from the surface, a regular etching pattern can be formed during etching dissolution, which was observed in the AFM etching images of both FFA I and FFA-TP CO faces shown in Figures. 4(b) and 4(g). Formation of the etching pattern on the crystal surface is determined by the crystal interaction network together with the interactions between solvent and crystal surface.<sup>17</sup> On the (100) face of FFA I, there are two non-perpendicular crystallographic axes: the *b*-axis and *c*-axis, in which the COOH or  $\text{CF}_3$  (see bottom) group in Figure 2 is exposed

out of the surface. Each molecule is surrounded by six neighbors, each attracted through  $\pi$ - $\pi$  stacking inside the surface, resulting in non-directional force along either the b-axis or c-axis. Therefore, the pits on the (100) face of FFA I were circular shape without specific preference of directions shown in Figure 4(b). Presumably, the size or strain of individual defects on the surface of FFA I was different before dissolution, leading to a wide size distribution of the pits. However, the situation is different for FFA-TP CO dissolution. When FFA-TP CO dissolves, both of FFA and TP molecules detach from the FFA-TP CO lattice from the defect sites on the surface. The different etching pattern in Figure 4(g) in comparison with that on the FFA I (100) face in Figure 4(b) reflects the more anisotropic nature of the interactions in FFA-TP CO, with the ditches roughly parallel to the strong hydrogen bonds. According to the single crystal dissolution experiments, linear dissolution rates were obtained for both the FFA-TP (001) and (100) faces, indicating that no solid form conversion occurred during dissolution [Figure 5(b5)]. Under non-sink conditions, the precipitation of FFA III solids was observed after 50 min [Figure 8(a)], when the FFA concentration in solution was above its solubility. Therefore a bulk precipitation mechanism is proposed for the FFA-TP CO dissolution, where the dissolved parent drug precipitates as individual crystals from the bulk solution, in contrast to a surface precipitation mechanism for the FFA-NIC CO dissolution, where the parent drug precipitates directly onto the surface of the dissolving cocrystals as a coating layer. The strong interaction between FFA and TP, along with the smaller difference in hydrophobicity between the coformers in FFA-TP CO relative to FFA-NIC CO, suggests that the coformers are more likely to remain closely associated in the case of FFA-TP CO. This would then lead to a smaller local supersaturation of FFA near the dissolving FFA-TP CO surface, thereby explaining the lack of surface precipitation.

When a polymer of PEG, PVP or PVP-VA was pre-dissolved in the dissolution medium, dissolution profiles of FFA-NIC CO or FFA-TP CO changed to significantly different extents

under either sink or non-sink conditions. In this study, the used polymer concentration of 200  $\mu\text{g/mL}$  was so low that the solution viscosity remained the same as that of the PBS dissolution medium alone. Furthermore, the pre-dissolved polymer had no effect on the solubility of FFA I [Table 2]. Therefore the effects of polymeric additives on the dissolution of FFA cocrystals are attributed to surface adsorption of the polymers through specific interactions with the crystal surface, in particular, hydrogen bonding.<sup>17-20,23,26,38,39</sup> Among the polymers used in this study, PEG, containing a high percentage of hydrogen acceptors in the backbone, is the most hydrophilic, while PVP-VA, containing 40% acetate side chains in comparison to PVP, is the most hydrophobic.<sup>11</sup>

Based on the dissolution experiment of the single FFA I crystal, the FFA I (100) face is more hydrophobic because it has a slower face dissolution rate in Figure 5(b1). The hydrophilic polymer of PEG with its rigid backbone chains should not be easily absorbed on the crystal surface. Therefore that there was no change of the etching patterns of FFA I (100) face in PBS in the presence of pre-dissolved PEG in Figure 4(c). Bigger and steeper pits observed were most likely caused by an enhanced diffusion rate of FFA molecules from the crystal surface attracted by PEG in solution due to less hydrophilic environment generated than water around the surface, indicating a slightly increased surface dissolution rate in the single crystal dissolution measurement in Figure 6. PVP and PVP-VA have oxygen molecules at the side chain positions, therefore, there should be no strong steric repulsion for them to form hydrogen bonds with the COOH groups of FFA I on the crystal surface. Once the polymers were adsorbed onto the surface, they prevented the dissolution medium contacting the crystal surface to retard the etching locally, leading smaller and less deep pits in Figures. 4(d) and 4(e). A lower density of the pits with irregular etching patterns in PBS in the presence PVP-VA [Figure 4(e)] indicated that PVP-VA had more chance to be adsorbed

on the FFA I crystal surface due to more oxygen molecules at the side chains in comparison with PVP.

The hydrophobic nature of the FFA-TP CO (001) face was likely to prevent PEG to be adsorbed on it; therefore, there was no change of the surface etching patterns in comparison with those in PBS alone in Figures. 4(g)-(h). With increasing the non-polarity of PVP and PVP-VA, both of the polymers had more opportunities to be adsorbed on the crystal surface, affecting the etching patterns of the FFA-TP (001) face in Figures 4(i)-(j) and also causing a reduction of the face dissolution rates in the single crystal face dissolution experiments in Figure 6 and decreased DPP values in the power dissolution experiments in Figure 7(e) and Figure 8(e). It has to be stressed that PVP or PVP-VA not only decreased the dissolution rates of FFA-TP CO but also prevented the precipitation of FFA III when the FFA concentration was above its solubility through intermolecular interaction in solution without increasing the solubility of FFA I,<sup>11</sup> confirmed by the PXRD results of the solid residues where FFA-TP COs were the only solid phase in Figure 9(b). Consequently an increased  $C_{max}$  in Table 5 was generated by the FFA-TP CO dissolution.

In the presence of PEG in PBS, the FFA-NIC (01-1) face dissolution rate increased and its (100) face dissolution rate reduced in Figure 5(b10), therefore there was no change of the overall dissolution performance of FFA-NIC CO in the bulk dissolution experiments in Figures. 7(e) and 8(e). In contrast, both PVP and PVP-VA were easily adsorbed on the FFA-NIC CO surface to slow down the crystal dissolution rate. Consequently precipitation rate of the stable form FFA III solids on the surface of the dissolving cocrystals was reduced, showing a similar roughness of the etching FFA-NIC (01-1) in the pre-dissolved PVP or PVP-VA as the original one prior to the etching experiment. Therefore the advantages of the improved solubility and dissolution rates of FFA-NIC CO were observed in the single crystal dissolution experiments in Figures 5(b11)-(b12) and bulk dissolution experiments in Figure

7(e) and Figure 8(e). It is worth re-emphasising that the precipitation of the stable form FFA III was only partially inhibited by the pre-dissolved PVP or PVP-VA in solution, supported by the evidence of the nonlinear face dissolution rates in Figures 5(b11)-(b12) and PXRD results of solid residues after non-sink powder experiments in Figure 9(c). Except the surface roughness, no change of the appearance of the FFA-NIC (01-1) face after etching dissolution shown in Figures 4(i)-(o) is another evidence to support the surface layer removal dissolution mechanisms of FFA-NIC CO. In order to maximize the advantages of FFA-NIC CO, an increasing polymer concentration or new approaches have to be developed to completely inhibit the FFA precipitation, which is part of on-going research in our group.

## 5. CONCLUSIONS

Understanding the dissolution mechanisms of pharmaceutical cocrystals can lead to strategies for improving cocrystal design and its optimum product development. In this study, effects of the three polymers, PEG, PVP and PVP-VA, on the dissolution behaviour of the cocrystals of FFA-TP CO and FFA-NIC CO were investigated at multiple length scales. At the molecular level, the interactions of a crystal surface with a polymer by observing etching pattern changes using AFM. At the macroscopic scale, dissolution rates of particular faces of a single crystal were determined by measurement of the physical retreat velocities of the faces using OLM. In the bulk experiments, the FFA concentration in a dissolution medium in the absence or presence of a polymer was measured under both sink and non-sink conditions. It has been found that the dissolution mechanisms of FFA-TP CO are controlled by the defect sites of the crystal surface and by precipitation of the parent drug as individual crystals in the bulk fluid. In contrast, the dissolution mechanisms of FFA-NIC CO are controlled by the surface layer removal and by a surface precipitation mechanism, where the parent drug precipitates directly onto the surface of the dissolving cocrystals as a coating layer. Through controlling the dissolution environment by pre-dissolving a polymer, PVP or PVP-VA, which can interact

with the crystal surface to alter its dissolution properties, the advantages of the improved solubility and dissolution rates of the FFA-TP CO and FFA-NIC CO can be demonstrated.

## ASSOCIATED CONTENT

### Supporting information

- 1) **Table S1.** Crystal structure data and details of refinements.
- 2) **Figure S1.** Characterisation of single crystals: (a) PXRD pattern; (b) IR spectra; (c) DSC thermographs.
- 3) **Figure S2.** Characterisation of solid residues after FFA I equilibrium experiments in PBS in the absence or presence of 200 µg/mL polymer of PEG, PVP or PVP-VA: (a) PXRD patterns; (b) IR spectra; (c) DSC thermographs.
- 4) **Figure S3.** Characterisation of solid residues after the tests in TP solutions: (a) DSC thermographs; (b) FTIR results;
- 5) **Figure S4.** Characterisation of solid residues after the tests in NIC solutions: (a) DSC thermographs; (b) FTIR results
- 6) **Figure S5.** AFM images
- 7) **Figure S6.** Three dimensional AFM images at a 40x40 µm<sup>2</sup> scan area
- 8) **Figure S7.** OLM images
- 9) **Figure S8.** DSC thermographs characterization of solid residues after un-sink condition dissolution: (a) FFA; (b) FFA-NIC CO; (C) FFA-TP CO.
- 10) **Figure S9.** FTIR results of solid residues after un-sink condition dissolution: (a) FFA; (b) FFA-NIC CO; (C) FFA-TP CO.

## AUTHOR INFORMATION

### Corresponding Author

\*E-mail: mli@dmu.ac.uk; Tel: +44-1162577132.

### Notes

The authors declare no competing financial interest.

## ACKNOWLEDGEMENTS

We would like to thank Dr. David Armitage from De Montfort University for supporting AFM measurements and Dr. Simon Roberts from Ashland Specialty Ingredients for providing materials for this study. De Montfort University and the Great Britain-China Educational Trust are gratefully acknowledged for providing scholarships for Miss Minshan Guo to conduct her PhD study. Dr. Ning Qiao would like to thank Science and Technology Project of Hebei Province (NO. 16211505) for supporting her to be involved in the work.

## REFERENCES

1. Qiao N, Li M, Schlindwein W, Malek N, Davies A, Trappitt G 2011. Pharmaceutical cocrystals: An overview. *International Journal of Pharmaceutics* 419(1–2):1-11.
2. Duggirala NK, Perry ML, Almarsson O, Zaworotko MJ 2016. Pharmaceutical cocrystals: along the path to improved medicines. *Chemical Communications* 52(4):640-655.
3. Kuminek G, Cao F, Bahia de Oliveira da Rocha A, Gonçalves Cardoso S, Rodríguez-Hornedo N 2016. Cocrystals to facilitate delivery of poorly soluble compounds beyond-rule-of-5. *Advanced Drug Delivery Reviews* 101:143-166.
4. Babu NJ, Nangia A 2011. Solubility Advantage of Amorphous Drugs and Pharmaceutical Cocrystals. *Crystal Growth & Design* 11(7):2662-2679.
5. Qiao N, Wang K, Schlindwein W, Davies A, Li M 2013. In situ monitoring of carbamazepine–nicotinamide cocrystal intrinsic dissolution behaviour. *European Journal of Pharmaceutics and Biopharmaceutics* 83(3):415-426.
6. Greco K, Bogner R 2012. Solution-Mediated Phase Transformation: Significance During Dissolution and Implications for Bioavailability. *Journal of Pharmaceutical Sciences* 101(9):2996-3018.
7. Yamashita H, Sun CC 2016. Harvesting Potential Dissolution Advantages of Soluble Cocrystals by Depressing Precipitation Using the Common Coformer Effect. *Crystal Growth & Design* 16(12):6719-6721.

8. Li M, Qiao N, Wang K 2013. Influence of Sodium Lauryl Sulfate and Tween 80 on Carbamazepine–Nicotinamide Cocrystal Solubility and Dissolution Behaviour. *Pharmaceutics* 5(4):508.
9. Li M, Qiu S, Lu Y, Wang K, Lai X, Rehan M 2014. Investigation of the Effect of Hydroxypropyl Methylcellulose on the Phase Transformation and Release Profiles of Carbamazepine-Nicotinamide Cocrystal. *Pharm Res* 31(9):2312-2325.
10. Qiu S, Lai J, Guo M, Wang K, Lai X, Desai U, Juma N, Li M 2016. Role of polymers in solution and tablet-based carbamazepine cocrystal formulations. *CrystEngComm* 18(15):2664-2678.
11. Guo M, Wang K, Hamill N, Lorimer K, Li M 2016. Investigating the Influence of Polymers on Supersaturated Flufenamic Acid Cocrystal Solutions. *Molecular Pharmaceutics* 13(9):3292-3307.
12. Shete A, Murthy S, Thorat B, Yadav A, Sajane S, Sakhare S, Doijad R 2017. Studies on effect of hydrophilic polymers on physicochemical properties of itraconazole cocrystals. *Future Journal of Pharmaceutical Sciences*.
13. Ullah M, Ullah H, Murtaza G, Mahmood Q, Hussain I 2015. Evaluation of Influence of Various Polymers on Dissolution and Phase Behavior of Carbamazepine-Succinic Acid Cocrystal in Matrix Tablets. *BioMed Research International* 2015:10.
14. Xu S, Dai W-G 2013. Drug precipitation inhibitors in supersaturable formulations. *International Journal of Pharmaceutics* 453(1):36-43.
15. Warren DB, Benameur H, Porter CJH, Pouton CW 2010. Using polymeric precipitation inhibitors to improve the absorption of poorly water-soluble drugs: A mechanistic basis for utility. *Journal of Drug Targeting* 18(10):704-731.
16. Wurster DE, Taylor PW 1965. Dissolution rates. *Journal of Pharmaceutical Sciences* 54(2):169-175.
17. Wen H, Li T, Morris KR, Park K 2004. How Solvents Affect Acetaminophen Etching Pattern Formation: Interaction between Solvent and Acetaminophen at the Solid/Liquid Interface. *The Journal of Physical Chemistry B* 108(7):2270-2278.
18. Wen H, Morris KR, Park K 2008. Synergic Effects of Polymeric Additives on Dissolution and Crystallization of Acetaminophen. *Pharm Res* 25(2):349-358.
19. Li T, Morris KR, Park K 2000. Influence of Solvent and Crystalline Supramolecular Structure on the Formation of Etching Patterns on Acetaminophen Single Crystals: A Study with Atomic Force Microscopy and Computer Simulation. *The Journal of Physical Chemistry B* 104(9):2019-2032.
20. Vasil'chenko MA, Shakhtshneider TP, Naumov DY, Boldyrev VV 1996. Topochemistry of the initial stages of the dissolution of single crystals of acetaminophen. *Journal of Pharmaceutical Sciences* 85(9):929-934.
21. Plomp M, van Enkevort WJP, Vlieg E 2000. Etching and surface termination of K<sub>2</sub>Cr<sub>2</sub>O<sub>7</sub> {0 0 1} faces observed using in situ atomic force microscopy. *Journal of Crystal Growth* 216(1–4):413-427.
22. Danesh A, Connell SD, Davies MC, Roberts CJ, Tendler SJB, Williams PM, Wilkins MJ 2001. An In Situ Dissolution Study of Aspirin Crystal Planes (100) and (001) by Atomic Force Microscopy. *Pharm Res* 18(3):299-303.
23. Wen H, Morris KR, Park K 2005. Hydrogen bonding interactions between adsorbed polymer molecules and crystal surface of acetaminophen. *Journal of Colloid and Interface Science* 290(2):325-335.
24. Wen H, Morris KR, Park K 2005. Study on the Interactions Between Polyvinylpyrrolidone (PVP) and Acetaminophen Crystals: Partial Dissolution Pattern Change. *Journal of Pharmaceutical Sciences* 94(10):2166-2174.
25. Kramarenko EY, Winkler RG, Khalatur PG, Khokhlov AR, Reineker P 1996. Molecular dynamics simulation study of adsorption of polymer chains with variable degree of rigidity. I. Static properties. *The Journal of Chemical Physics* 104(12):4806-4813.
26. Bukovec P, Meden A, Smrkolj M, Vrečer F. 2015. Influence of crystal habit on the dissolution of simvastatin single crystals. ed.

27. Prasad KVR, Ristic RI, Sheen DB, Sherwood JN 2002. Dissolution kinetics of paracetamol single crystals. *International Journal of Pharmaceutics* 238(1–2):29-41.
28. Raghavan SL, Ristic RI, Sheen DB, Sherwood JN Dissolution Kinetics of Single Crystals of  $\alpha$ -Lactose Monohydrate. *Journal of Pharmaceutical Sciences* 92(2):439.
29. Snyder RC, Doherty MF 2007. Faceted crystal shape evolution during dissolution or growth. *AIChE Journal* 53(5):1337-1348.
30. Snyder RC, Veessler S, Doherty MF 2008. The Evolution of Crystal Shape During Dissolution: Predictions and Experiments. *Crystal Growth & Design* 8(4):1100-1101.
31. Good DJ, Rodríguez-Hornedo N 2009. Solubility Advantage of Pharmaceutical Cocrystals. *Crystal Growth & Design* 9(5):2252-2264.
32. Delaney SP, Smith TM, Korter TM 2014. Conformational origins of polymorphism in two forms of flufenamic acid. *Journal of Molecular Structure* 1078:83-89.
33. Fábíán L, Hamill N, Eccles KS, Moynihan HA, Maguire AR, McCausland L, Lawrence SE 2011. Cocrystals of Fenamic Acids with Nicotinamide. *Crystal Growth & Design* 11(8):3522-3528.
34. Aitipamula S, Wong ABH, Chow PS, Tan RBH 2014. Cocrystallization with flufenamic acid: comparison of physicochemical properties of two pharmaceutical cocrystals. *CrystEngComm* 16(26):5793-5801.
35. López-Mejías V, Kampf JW, Matzger AJ 2012. Nonamorphism in Flufenamic Acid and a New Record for a Polymorphic Compound with Solved Structures. *Journal of the American Chemical Society* 134(24):9872-9875.
36. Putra OD, Umeda D, Nugraha YP, Furuishi T, Nagase H, Fukuzawa K, Uekusa H, Yonemochi E 2017. Solubility improvement of epalrestat by layered structure formation via cocrystallization. *CrystEngComm* 19(19):2614-2622.
37. Hu Y, Liang JK, Myerson AS, Taylor LS 2005. Crystallization Monitoring by Raman Spectroscopy: Simultaneous Measurement of Desupersaturation Profile and Polymorphic Form in Flufenamic Acid Systems. *Industrial & Engineering Chemistry Research* 44(5):1233-1240.
38. Wen H, Li T, Morris KR, Park K 2004. Dissolution Study on Aspirin and  $\alpha$ -Glycine Crystals. *The Journal of Physical Chemistry B* 108(30):11219-11227.
39. Li T, Morris KR, Park K 2001. Influence of Tailor-Made Additives on Etching Patterns of Acetaminophen Single Crystals. *Pharm Res* 18(3):398-402.

Table 1: Chemical structures of model drug, coformers, and nonomer units of polymers

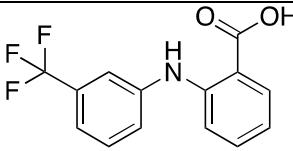
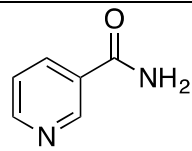
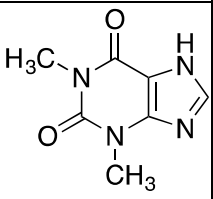
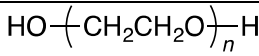
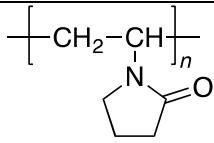
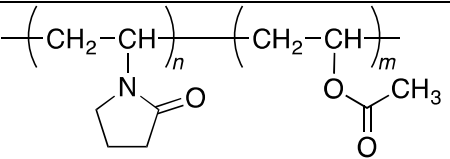
	FFA	NIC	TP	PEG	PVP	PVP-AV
Molecular structure						

Table 2: Solubility test results

FFA I equilibrium solubility ( $\mu\text{g/mL}$ )	In PBS	373.3 $\pm$ 4.2
	In PBS with pre-dissolved PEG	376.3 $\pm$ 6.7
	In PBS with pre-dissolved PVP	387.7 $\pm$ 5.9
	In PBS with Pre-dissolved PVP-VA	398.8 $\pm$ 2.3
FFA-TP cocrystal transition concentration ( $\mu\text{g/mL}$ )	FFA concentration in 8.9 mM of TP solution	439.9 $\pm$ 2.0
	TP concentration in 8.9 mM of TP solution	1028.9 $\pm$ 25.3
FFA-NIC cocrystal transition concentration ( $\mu\text{g/mL}$ )	FFA concentration in 66.8 mM of NIC solution	474.3 $\pm$ 15.6
	NIC concentration in 66.8 mM of NIC solution	7812.5 $\pm$ 300.6

Table 3: AFM measurements

Crystal	Face	Dissolution time (min)			
		PBS	PBS with pre-dissolved PEG	PBS with pre-dissolved PVP	PBS with pre-dissolved PVP-VA
FFA I	(100)	10	10	10	10
FFA-TP CO	(001)	10	10	10	10
FFA-NIC CO	(01-1)	2	2	3	4

Table 4:  $T_{equilibrium}$  values of powder dissolution under non-sink conditions

Crystal	$T_{equilibrium}$ (min)			
	PBS	PBS with pre-dissolved PEG	PBS with pre-dissolved PVP	PBS with pre-dissolved PVP-VA
FFA I	166	196	>240	186
FFA-TP CO	50	10	62	87
FFA-NIC CO	223	196	23	22

Table 5:  $C_{max}$  values of powder dissolution under non-sink conditions

Crystal	$C_{max}$ ( $\mu\text{g/mL}$ )			
	PBS	PBS with pre-dissolved PEG	PBS with pre-dissolved PVP	PBS with pre-dissolved PVP-VA
FFA I	415.3 $\pm$ 6.0	397.8 $\pm$ 8.40	283.3 $\pm$ 44.8	415.4 $\pm$ 32.8
FFA-TP CO	497.5 $\pm$ 20.7	527.1 $\pm$ 23.3	538.8 $\pm$ 32.9	539.4 $\pm$ 1.6
FFA-NIC CO	383.6 $\pm$ 34.1	397.3 $\pm$ 20.7	609.4 $\pm$ 14.0	629 $\pm$ 10.1

Fig. 1: Illustration of dissolution performance parameter

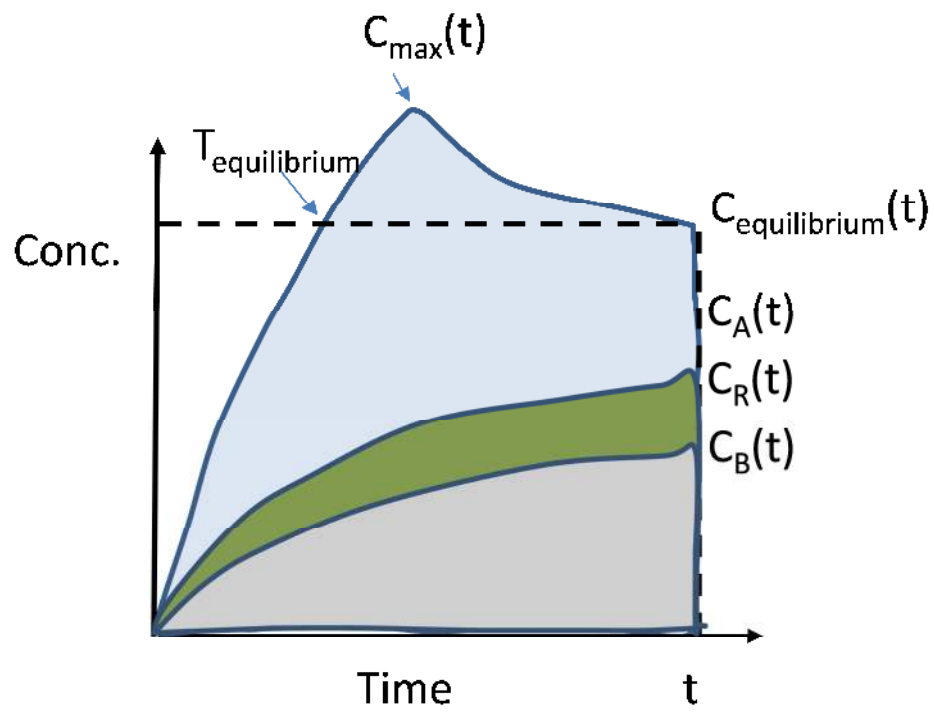
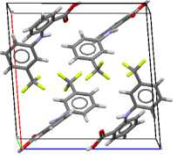
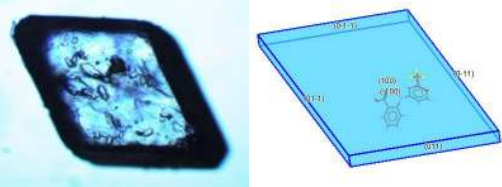
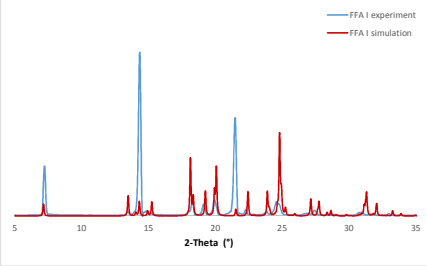
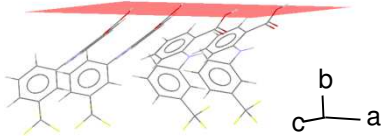
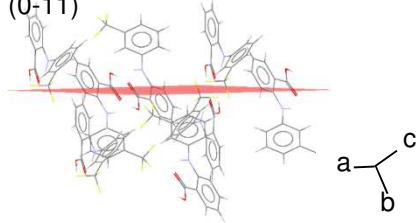
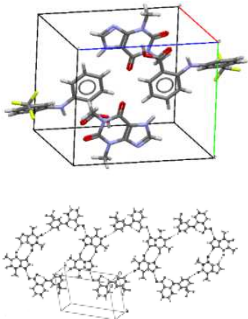
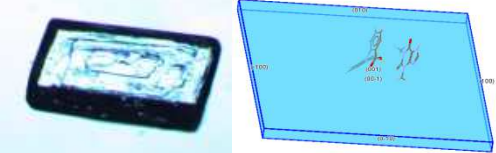
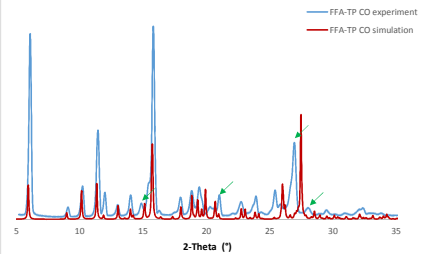
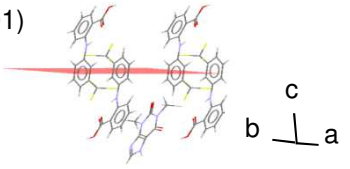
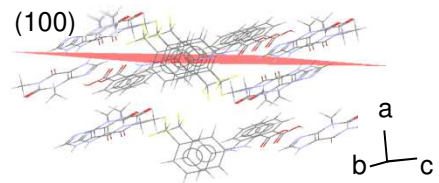


Figure 2: Crystal morphologies and molecular packings at crystal faces used in experiments.

Crystal	Unit cell & supramolecular network	Comparison of predicted morphology and PXRD with measurements	Structure of crystal face	
			Structure of each face	Functional group exposed on plane
FFA I		 	(100) 	COOH (see top) or CF <sub>3</sub> (see bottom)
			(0-11) 	CF <sub>3</sub> , COOH, and the aromatic rings of FFA
FFA-TP CO		 	(001) 	COOH, aromatic rings and CF <sub>3</sub> (both FFA) or COOH (FFA) and NH and C=O (TP)
			(100) 	Plane is approximately parallel with <b>mean</b> plane of molecules, so can expose any part of the molecules on the surface

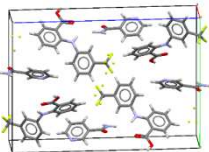
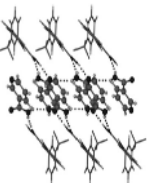
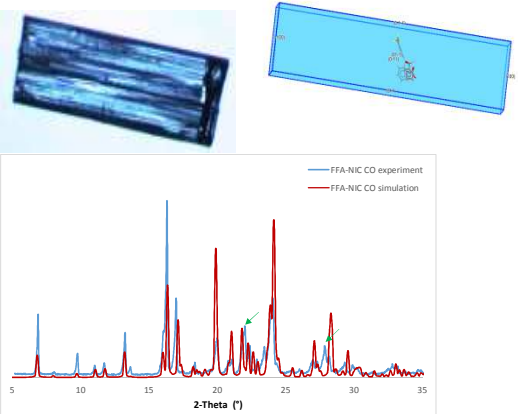
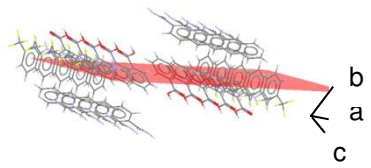
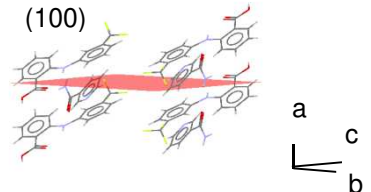
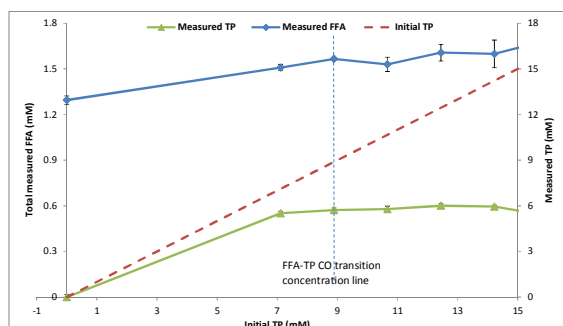
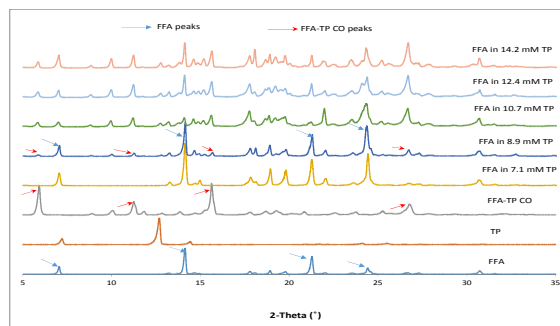
FFA-NIC CO	 		<p>(01-1)</p> 	Aromatic rings (both molecules) and CF <sub>3</sub> or aromatic rings, amide and pyridine N (NIC)
			<p>(100)</p> 	CF <sub>3</sub> and aromatic rings with COOH and NH

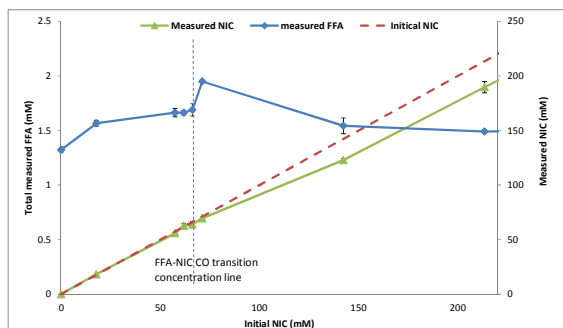
Fig. 3: Apparent solubility of FFA I in a coformer solution: (a) FFA and TP concentrations as a function of TP concentration; (b) PXRD results of solid residues after the tests in TP solutions; (c) FFA and NIC concentrations as a function of NIC concentration; (d) ) PXRD results of solid residues after the tests in NIC solutions



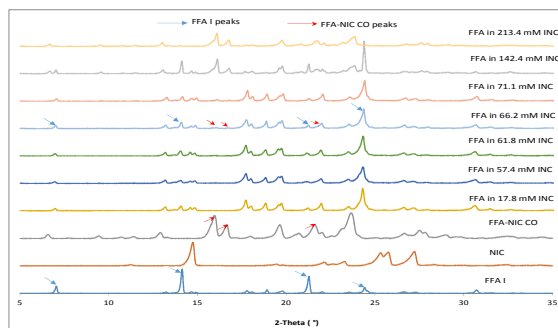
(a)



(b)



(c)



(d)

Fig. 4: AFM images of results at a  $40 \times 40 \mu\text{m}^2$  scan area

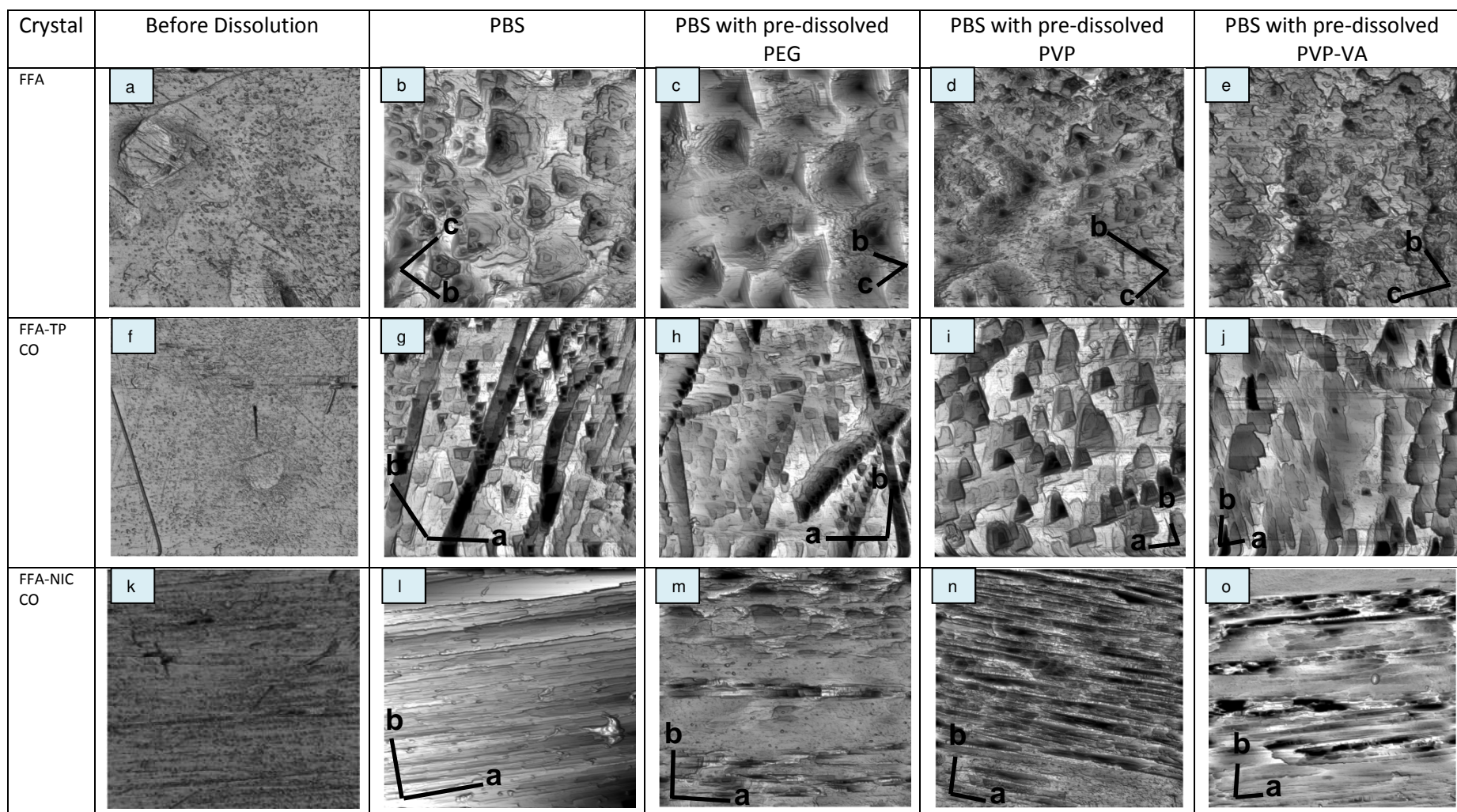
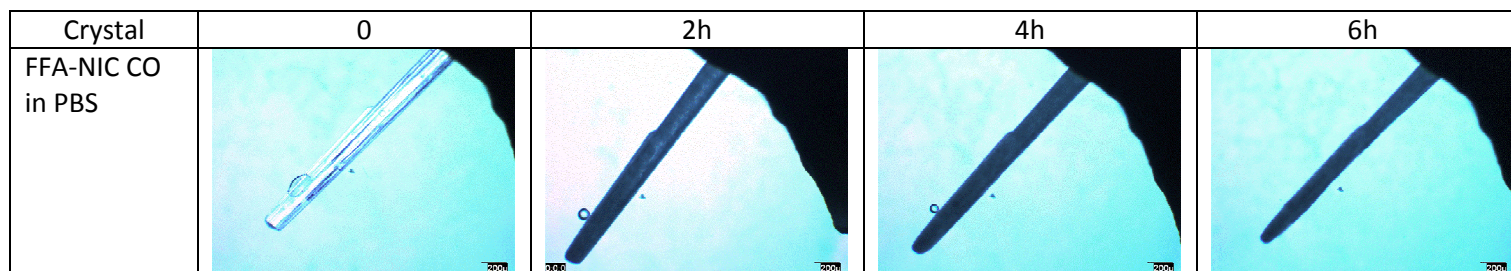
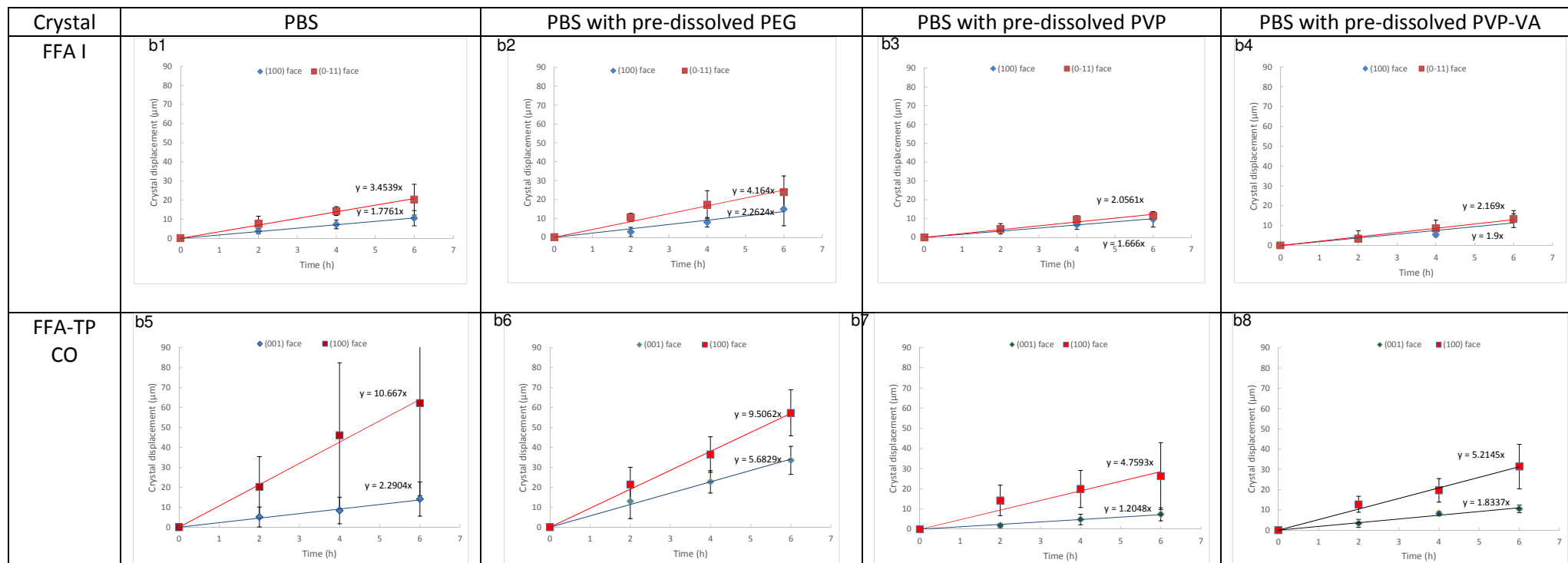


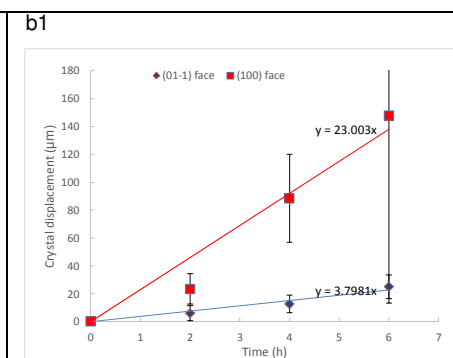
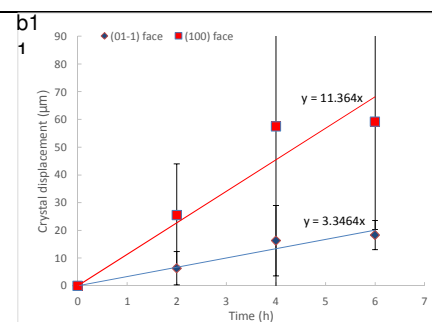
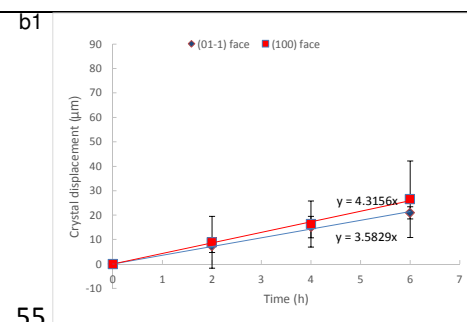
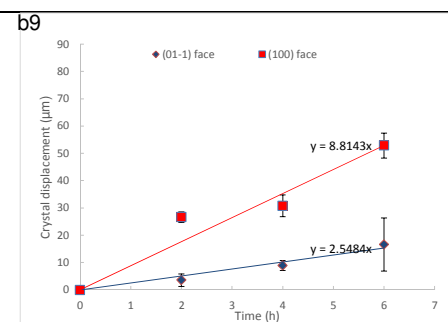
Fig. 5: OLM dissolution experiments: a) representative OLM images of single crystal during dissolution; b) displacements of the edge of a crystal face as a function of dissolution time



(a)



FFA-NIC  
CO



555

(b)

**Figure 6.** Face dependent dissolution rate of a single crystal in PBS in the absence and presence of a polymer.

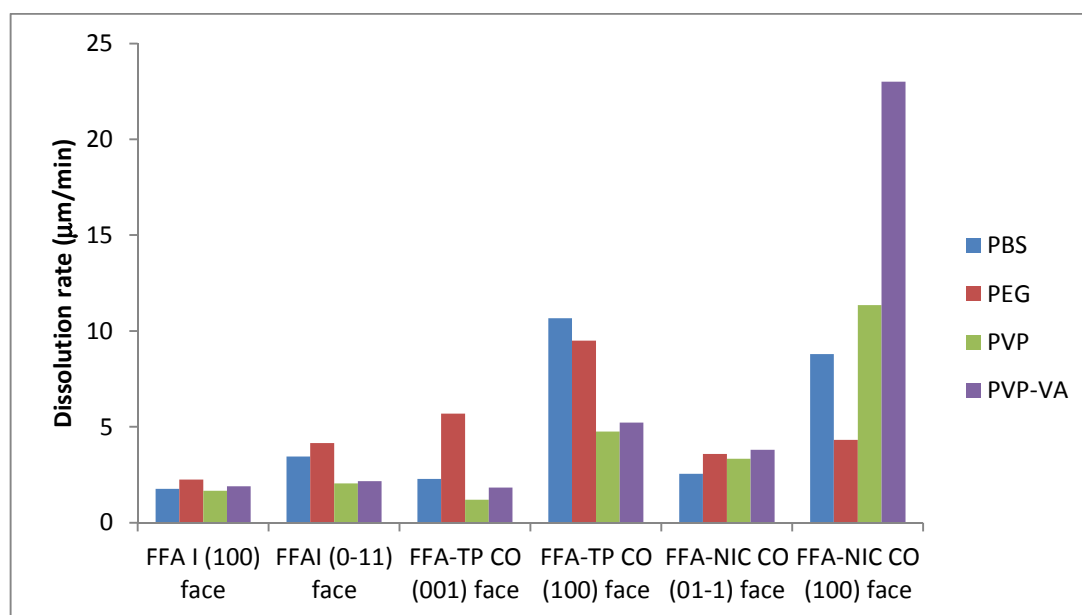


Fig. 7: Powder dissolution profiles in the absence or presence of a polymer under sink conditions: (a) PBS; (b) PBS with pre-dissolved PEG; (c) PBS with pre-dissolved PVP; (d) PBS with pre-dissolved PVP-VA

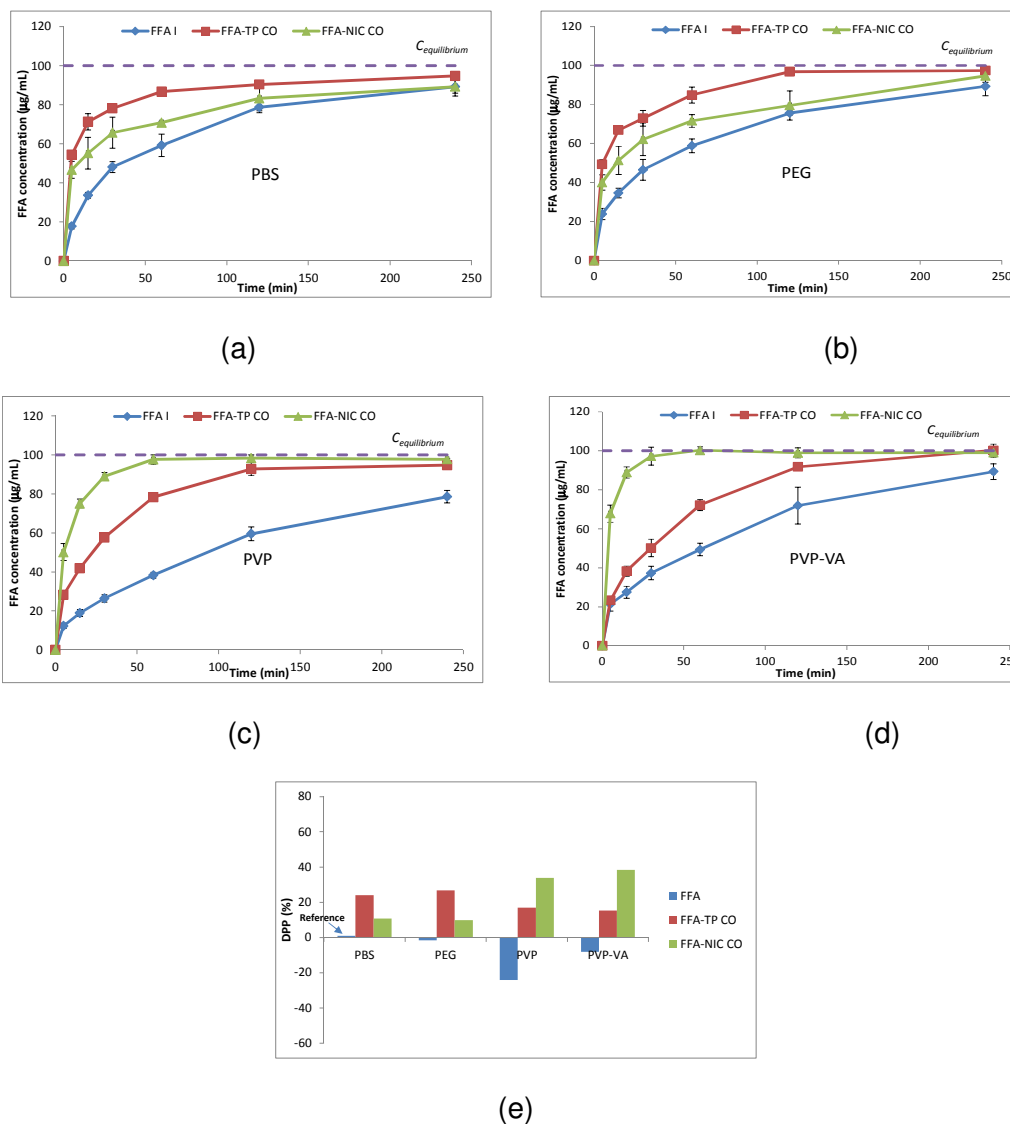
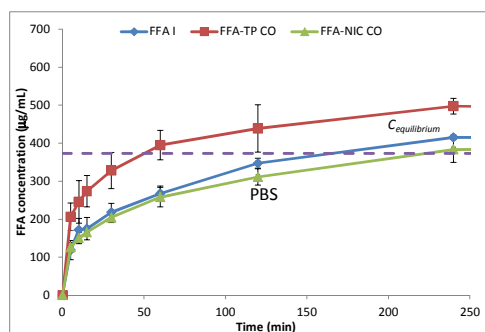
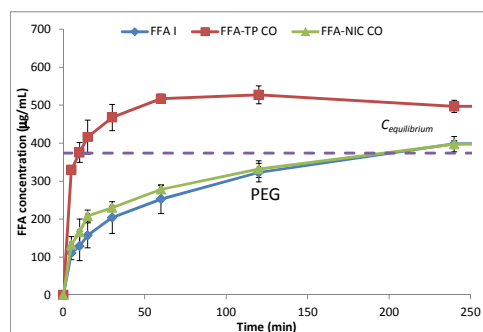


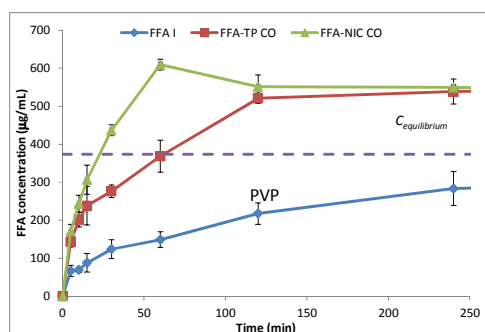
Fig. 8: Powder dissolution profiles in the absence or presence of a polymer under non-sink conditions: (a) PBS; (b) PBS with pre-dissolved PEG; (c) PBS with pre-dissolved PVP; (d) PBS with pre-dissolved PVP-VA



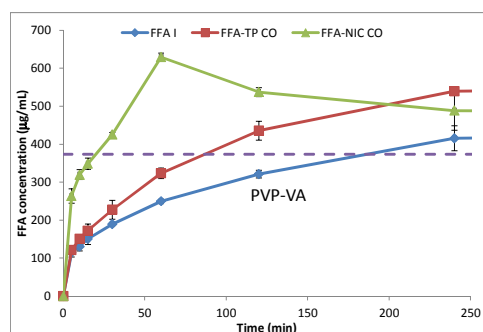
(a)



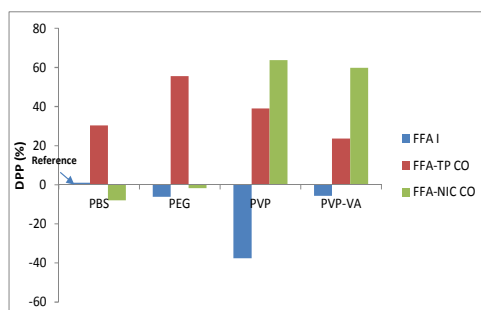
(b)



(c)

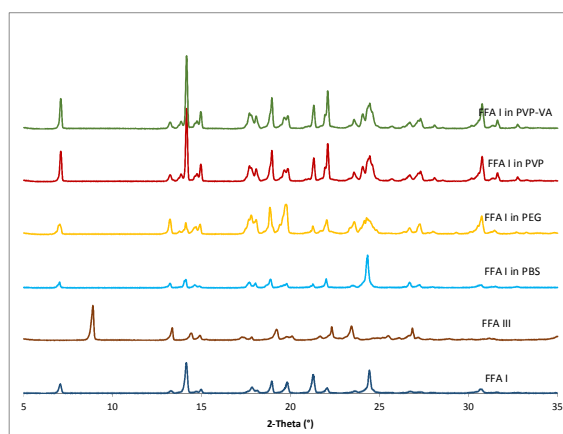


(d)

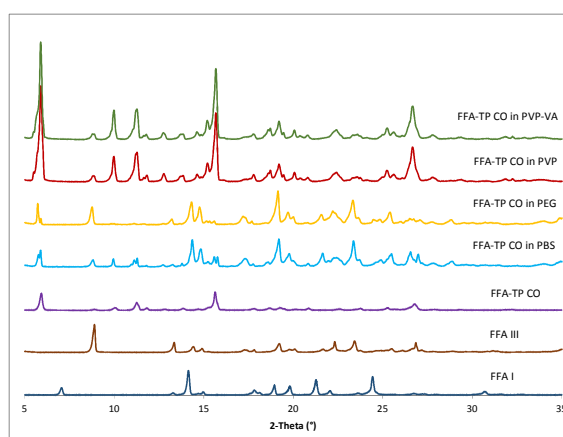


(e)

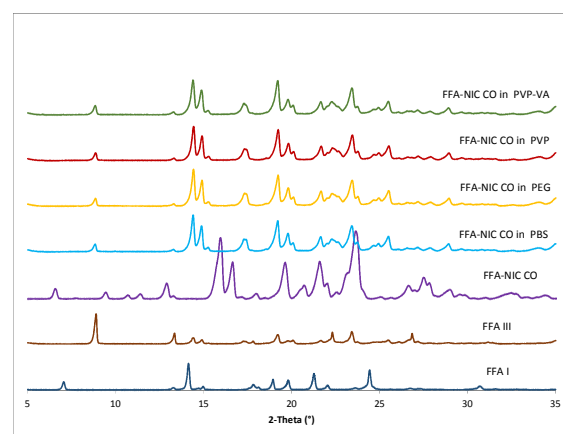
Fig. 9: Test results of solid residues after dissolution tests under non-sink conditions: (a) FFA I; (b) FFA-TP CO (c) FFA-NIC CO



(a)



(b)



(c)